INTERNATIONAL JOURNAL FOR NUMERICAL METHODS IN FLUIDS
Int. J. Numer. Meth. Fluids 2002; **39**:1–22 (DOI: 10.1002/fld.233)

Application of moving adaptive grids for numerical solution of 2D nonstationary problems in gas dynamics

Sergey A. Ivanenko*,† and Boris N. Azarenok

Computing Center of Russian Academy of Science, Vavilov str. 40, GSP-1, Moscow, 117967, Russia

SUMMARY

Solution-adaptive grid generation procedure is coupled with the Godunov-type solver of the second-order accuracy. Dynamically adaptive grids, clustered to singularities, allow to increase the accuracy of numerical solution. The theory of harmonic maps is used as a theoretical framework for grid generation. The problem of constructing harmonic coordinates on the surface of the graph of control function is formulated. The projection of these coordinates onto a physical domain produces an adaptive-harmonic structured grid. A variational grid generator which can be used also in the case of unstructured grids with adaptation to a vector-function is described in detail. The discrete functional has an infinite barrier on the boundary of the set of grids with all convex cells and this guarantees unfolded grid generation at every time step. Results of test computations are presented. Copyright © 2002 John Wiley & Sons, Ltd.

KEY WORDS: gas dynamics; supersonic flow; high-order scheme; adaptive grid; harmonic mapping; unfolded grid

1. INTRODUCTION

The main purpose of the present work is to investigate the possibility of applying the method of adaptive-harmonic grid generation, which has shown essential advantages in the stationary problems [1–3], to the nonstationary problems of gas dynamics.

It is well known that grid adaptation to singularities of the numerical solution allows to increase greatly the accuracy of computations [4]. However, there are some additional numerical problems here. It is necessary to obtain a correct resolution of singularities and suppress nonphysical spurious oscillations. In the present paper the method of adaptive grid generation, based on the theory of harmonic maps, ensuring generation of unfolded grids at every time step is presented. The method is variational, i.e. we consider the problem of minimizing

*Correspondence to: S. A. Ivanenko, Computing Center of Russian Academy of Science, Vavilov str. 40, GSP-1, Moscow, 117967, Russia.
† E-mail: sivan@ccas.ru

The work was supported by the Russian Foundation for Basic Research, project no. 99-01-00264.

Received June 2000
Revised March 2001

a finite-difference function approximating the Dirichlet's functional written for surfaces. The discrete functional has an infinite barrier on the boundary of the set of grids with all convex cells and this guarantees unfolded grid generation during computations. This folding-resistant property is very important in nonstationary problems since if any of the cells become folded we have to stop the calculation and use special procedures to continue modeling.

Although in the paper we present results obtained on structured grids, the method can be extended to unstructured grids as well.

Moving grid techniques have been developed in a number of works [5–9]. All these methods, in contrast to those presented in this paper, do not ensure the generated grids to be unfolded at discrete level.

To execute calculations on the moving curvilinear grids a Godunov Linear Fluxes Correction (GLFC) scheme is used, being a modification of the Godunov scheme with fluxes correction and time splitting, that provides the second-order accuracy in time and space to the smooth solutions [10]. In order to suppress nonphysical spurious oscillations in the vicinity of the discontinuities a monotonicity algorithm is applied.

2. FLOW SOLVER

In this section we shall briefly describe the GLFC scheme used as a flow solver [10].

We write the variational formulation for the hyperbolic system of gas dynamics equations in integral form of conservation laws

$$\oiint_A \boldsymbol{\sigma}\,\mathrm{d}x\,\mathrm{d}y + \boldsymbol{a}\,\mathrm{d}y\,\mathrm{d}t + \boldsymbol{b}\,\mathrm{d}t\,\mathrm{d}x = \mathbf{0} \tag{1}$$

where

$$\boldsymbol{\sigma} = \begin{bmatrix} \rho \\ \rho u \\ \rho v \\ E \end{bmatrix}, \quad \boldsymbol{a} = \begin{bmatrix} \rho u \\ \rho u^2 + p \\ \rho uv \\ u(E+p) \end{bmatrix}, \quad \boldsymbol{b} = \begin{bmatrix} \rho v \\ \rho uv \\ \rho v^2 + p \\ v(E+p) \end{bmatrix}$$

here u and v are the velocity components, p and ρ are the pressure and density. Total energy $E = \rho[e + 0.5(u^2 + v^2)]$, here e is the specific internal energy. Equation of state is $p = (\gamma - 1)\rho e$, where γ is the ratio of specific heats. Denote the vector of unknown functions as $\boldsymbol{f} = (u, v, p, \rho)^T$.

Let us introduce the curvilinear moving grid in space $x - y - t$ (see Figure 1(a)). Bottom face of the computing cell (or control volume) is taken at time level n and the top face at level $n + 1$.

Integrating in Equation (1) over the oriented surface being the boundary of the control volume we obtain a cell-centered finite-volume discretization of the governing equations

$$\boldsymbol{\sigma}^{n+1}\boldsymbol{A}^{n+1} - \boldsymbol{\sigma}^n\boldsymbol{A}^n + \boldsymbol{Q}_{11'4'4} + \boldsymbol{Q}_{233'2'} + \boldsymbol{Q}_{122'1'} + \boldsymbol{Q}_{433'4'} = \mathbf{0} \tag{2}$$

where $\boldsymbol{\sigma}^{n+1}$ and $\boldsymbol{\sigma}^n$ are the average values at time t^{n+1} and t^n in the center of the top and bottom faces, $\boldsymbol{A}^{n+1}$ and $\boldsymbol{A}^n$ are the areas of these faces. Each of four vector values

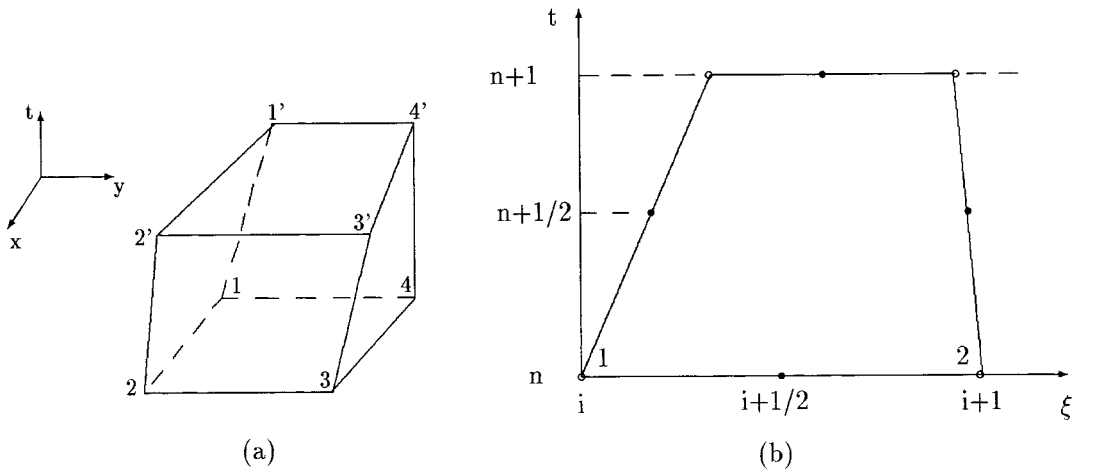

Figure 1. Computational cell.

$\boldsymbol{Q}_{11'4'4}$, $\boldsymbol{Q}_{233'2'}$, $\boldsymbol{Q}_{122'1'}$ and $\boldsymbol{Q}_{433'4'}$ is an average flux of mass, impulse and energy through the corresponding intercell surface towards the outward normal vector.

For example, to the face $122'1'$ the value $\boldsymbol{Q}_{122'1'}$ has the following structure

$$\boldsymbol{Q}_{122'1'} = \boldsymbol{\sigma}_{122'1'}\boldsymbol{A}^{xy}_{122'1'} + \boldsymbol{a}_{122'1'}\boldsymbol{A}^{yt}_{122'1'} + \boldsymbol{b}_{122'1'}\boldsymbol{A}^{tx}_{122'1'} \tag{3}$$

where $\boldsymbol{A}^{xy}_{122'1'}$, $\boldsymbol{A}^{yt}_{122'1'}$, $\boldsymbol{A}^{tx}_{122'1'}$ are the areas of projections of the face $122'1'$ onto the coordinate planes $x-y$, $y-t$ and $t-x$, respectively. In Equation (3) all values are defined in the center of the face $122'1'$ using the post-wave values after solving the Riemann problem. Pre-wave values $\boldsymbol{f}$ in the center of the face are obtained by time splitting and a special interpolation procedure that provides the scheme with the second-order accuracy in time and space in the domains of smooth solution.

In every cell the admissible time step $\Delta t_{i+1/2,j+1/2}$ is defined by [11]

$$\begin{aligned}
\Delta t'_{i+1/2,j+1/2} &= \frac{h'_{i+1/2,j+1/2}}{\max(D^{II}_{i,j+1/2} - W_{i,j+1/2}, -D^{I}_{i+1,j+1/2} - W_{i+1,j+1/2})} \\
\Delta t''_{i+1/2,j+1/2} &= \frac{h''_{i+1/2,j+1/2}}{\max(D^{II}_{i+1/2,j} - W_{i+1/2,j}, -D^{I}_{i+1/2,j+1} - W_{i+1/2,j+1})} \\
h'_{i+1/2,j+1/2} &= \frac{A_{1234}}{\sqrt{(x_{i+1,j+1/2} - x_{i,j+1/2})^2 + (y_{i+1,j+1/2} - y_{i,j+1/2})^2}} \\
h''_{i+1/2,j+1/2} &= \frac{A_{1234}}{\sqrt{(x_{i+1/2,j+1} - x_{i+1/2,j})^2 + (y_{i+1/2,j+1} - y_{i+1/2,j})^2}} \\
\Delta t_{i+1/2,j+1/2} &= \frac{\Delta t'_{i+1/2,j+1/2}\,\Delta t''_{i+1/2,j+1/2}}{\Delta t'_{i+1/2,j+1/2} + \Delta t''_{i+1/2,j+1/2}}
\end{aligned} \tag{4}$$

Here $\Delta t'$ and $\Delta t''$ are the admissible time steps to 1-D schemes, h', h'' are the 'average heights' of the bottom face A_{1234}, W is the velocity of the corresponding cell edge (e.g. $W_{i+1/2,j}$ is the velocity of the edge 12 which defines inclination of the face $122'1'$), see Figure 1(a). Next, for example, $D^{II}_{i,j+1/2}$ is the 'extreme right wave' speed in the ξ direction defined from solving the Riemann problem to the face $11'4'4$, and $D^{I}_{i+1,j+1/2}$ is the 'extreme left wave' speed in the ξ direction to the face $233'2'$. By analogy we get $D^{II}_{i+1/2,j}$ and $D^{I}_{i+1/2,j+1}$, the wave speeds in the η direction.

As an admissible time step we take the minimal $\Delta t_{i+1/2,j+1/2}$ of all cells of the grid

$$\Delta t = c_{cfl} \min_{i,j} \Delta t_{i+1/2,j+1/2} \tag{5}$$

The coefficient c_{cfl} is less than 1 (usually close to 1) and it is introduced as a correction to the nonlinearity of the problem. Note that the time step depends on both the post-wave values and velocity of every intercell face. In computations the value of Δt, obtained at the preceding time step, is used to the next time step. For this reason in the case of essentially nonstationary processes the coefficient should be greatly decreased.

3. UNFOLDED GRIDS

Two types of grids are used in computations: structured and unstructured. In structured grids the subsequent connections between points are defined automatically from the indexing. A typical example is a curvilinear grid constructed by a mapping of a parametric square onto a physical domain. Grid nodes are enumerated with double indices in the two-dimensional case. This is not the case of unstructured grids. For such a grid, neighbors of nodes must be specified.

The condition of the Jacobian positiveness of a mapping is used to derive conditions for a structured grid to be unfolded [2, 3]. An unstructured grid can be assumed as a set of local coordinates, so the condition of the Jacobian positiveness can be used also to derive conditions for an unstructured grid to be unfolded.

In the employment of unstructured grids we must define the correspondence between local (for each element) and global node enumeration. In Figure 2 the simplest example of an unstructured grid of four cells is shown. Element numbers are shown in circles. The local enumeration is shown only for the element 1. The global enumeration is shown with a bold font.

The correspondence between local and global node numbers is introduced as follows

$$n = n(N,k), \quad n = 1,\ldots,N_n, \;\; N = 1,\ldots,N_e, \;\; k = 1,2,3,4,$$

where n is the global node number, N_n is the total number of grid nodes, N is an element number, N_e is the number of elements, k is a local node number in the element. This correspondence is implemented in the computer program as a function for a structured grid and as an array for an unstructured grid. For example, for the unstructured grid shown in Figure 2 the correspondence between local and global enumeration is defined as follows

$$n(1,1) = 1, \quad n(1,2) = 3, \quad n(1,3) = 4, \quad n(1,4) = 2$$

For structured grids this correspondence is defined by simple formulae [2].

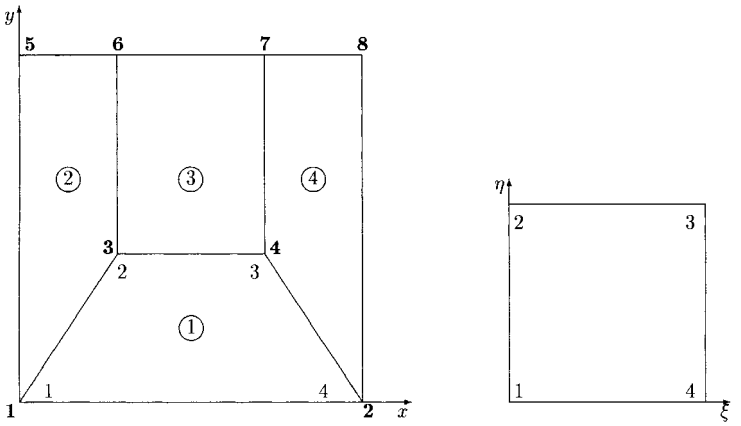

Figure 2. Correspondence of node numbers for a mapping of the unit square in the plane ξ, η onto the quadrilateral cell 1 of an unstructured mesh in the plane x, y.

Now we consider conditions for the grid node coordinates to assure a grid to be nondegenerate. Note, that in case of a structured grid instead of the mapping $x(\xi,\eta)$, $y(\xi,\eta)$ of the parametric rectangle onto a domain Ω, a bilinear mapping of the same unit square onto each quadrilateral cell can be considered (see Reference [2]). All argumentation will be true in this case, since the Jacobian of the mapping $x^h(\xi,\eta)$, $y^h(\xi,\eta)$ is not changed if the square cell is shifted in the plane ξ, η. Hence, for each cell of unstructured grid a bilinear mapping of the unit square in the plane ξ, η onto this cell can be introduced (see Figure 2). The condition of the Jacobian positiveness can be written as follows

$$[J_k]_N > 0, \quad k = 1,2,3,4; \;\; N = 1,\ldots,N_e \tag{6}$$

where $J_k = (x_{k-1} - x_k)(y_{k+1} - y_k) - (y_{k-1} - y_k)(x_{k+1} - x_k)$ is the doubled area of the triangle, written in local enumeration, index k is cyclic. Consequently, all grid cells with node coordinates, satisfying inequalities $J_k > 0$, $k = 1,2,3,4$ will be convex quadrilaterals.

Grids, satisfying inequalities (Equation (6)) will be called convex or unfolded grids and denoted by $\mathscr{D}$. This set is a subset of the Euclidean space $R^{N_{\text{in}}}$, where N_{in} is the total number of degrees of freedom of the grid equal to double the number of its internal nodes. In this space $\mathscr{D}$ is an open bounded set. Its boundary $\partial\mathscr{D}$ is the set of grids for which at least one of the inequalities (Equation (6)) becomes an equality.

4. PROBLEM FORMULATION FOR GRID GENERATION

To generate a structured adaptive-harmonic grid we formulate the problem of minimizing the harmonic (Dirichlet's) functional, written for a surface [1, 2]. Notations are shown in Figure 3.

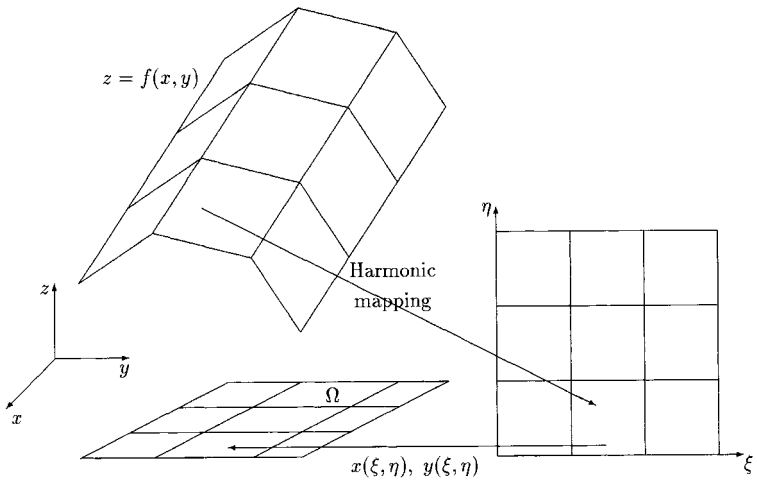

Figure 3. Harmonic coordinates on the surface of the graph of a function $z = f(x, y)$.

Let us consider the functional defining the adaptive-harmonic grid, clustered in regions of high gradients of the function $f(x, y)$

$$I = \int\int \frac{((1 + f_x^2)(x_\xi^2 + x_\eta^2) + 2f_x f_y(x_\xi y_\xi + x_\eta y_\eta) + (1 + f_y^2)(y_\xi^2 + y_\eta^2)}{(x_\xi y_\eta - x_\eta y_\xi)\sqrt{1 + f_x^2 + f_y^2}} \, d\xi \, d\eta \tag{7}$$

The problem of unstructured grid adaptation (r-refinement) is formulated as follows. Let the coordinates of the unstructured grid nodes be given. The grid is formed by quadrilateral elements only. The problem is to find new coordinates of the grid nodes minimizing the functional (Equation (7)) values computed for a mapping of the unit square onto every grid cell. In nonstationary problems such a formulation is considered at every time step and grid adaptation is performed to the control function considered as a function $f(x, y)$ at this time level.

The functional (Equation (7)) can be minimized both with given fixed location of the boundary nodes and when they move along the boundary. In the latter case new positions of the boundary points are obtained from the one-dimensional analog of the functional (Equation (7)), written for the boundary curve [12].

In order to control the number of grid nodes in the layer of high gradients, earlier it has been suggested to use the function $c_a f(x, y)$ instead of $f(x, y)$ [1, 2]. Here the function $f(x, y)$ is scaled so that the difference between maximal and minimal values of it is equal to the length of the diagonal of a rectangle enclosing all the boundary points that describe the geometry in the plane x, y, i.e.

$$f_{\max} - f_{\min} = \sqrt{(x_{\max} - x_{\min})^2 + (y_{\max} - y_{\min})^2}$$

The larger the coefficient of adaptation c_a the greater the number of grid nodes in the layer of high gradients. Usually c_a is in the range from 0.1 to 0.5. In the case of elliptic problems

the number of points in the layer is proportional to $c_a/(c_a+1)$, i.e. if $c_a = 0.5$ then about one third of the points is located in the layer of high gradients.

Note that if the algorithm of adaptive-harmonic grid generation is applied to the elliptic problems, it is assumed the function $f(x, y)$ to be continuously differentiable. If we solve the hyperbolic systems of gas dynamics, the function $f(x, y)$ can be discontinuous and in this case the coefficient c_a changes its essence. Numerical experiments show that in the case of adaptation to a smooth function, when increasing the coefficient c_a the grid begins 'to feel' new subdomains where the gradient is rather essential. Moreover, in Reference [1] it was shown that in the case of continuously differentiable function of one variable $f(x)$ in the limit of $c_a \to \infty$ we obtain a grid being optimal in norm L_∞ in a sense that the error of piecewise constant interpolation on such a grid in the norm L_∞ will be minimal. In fact, in 1-D case the functional (Equation (7)), in which the function $f(x)$ is changed to $c_a f(x)$ and f is scaled to be in the range $0 \leqslant f(x) \leqslant 1$, $x, \xi \in [0, 1]$, takes the form

$$I = \int \frac{1}{x_\xi \sqrt{1 + c_a^2 f_x^2}} \, \mathrm{d}\xi$$

and the Euler equation to this functional, defining behavior of the Jacobian of the adaptive-harmonic grid at the continuous limit, may be written as

$$x_\xi = \mathrm{const}(1/c_a^2 + f_x^2)^{-1/2}$$

It can be shown [1] if the grid is optimal in the norm L_∞ for piecewise constant interpolation, at the continuous limit the following expression for the Jacobian holds

$$x_\xi = \mathrm{const}\,|f_x|^{-1}$$

Hence, the adaptive-harmonic grid is optimal in the norm L_∞ at the limit $c_a \to \infty$.

From the above expressions for x_ξ it follows that if the function f is discontinuous, then, independently of the value $c_a > 0$ at adaptation, the cell size might approach zero in the vicinity of the discontinuity. Thus, it is necessary to modify the discontinuous function f in such a way that, firstly, to get a smooth function and, secondly, the regions of high gradients of the modified function would correspond to the discontinuities of the function f.

It can be achieved if, for example, to introduce an artificial viscosity or change problem formulation, i.e. instead of the Euler equations consider the Navier–Stokes equations. Here we use another approach based on introducing an additional parameter restricting the maximal value of the control function gradient. In such an approach the number of grid points in the vicinity of the shock should be limited and does not depend on c_a. Now c_a plays the following role: when increasing the coefficient c_a the grid begins 'to feel' the discontinuities of less intensity. Decrease of c_a results in decreasing sensitivity of the grid to the discontinuities of greater intensity and in the limit of $c_a = 0$ we obtain a quasiuniform harmonic grid not depending on $f(x, y)$.

Thus, the coefficient c_a is only responsible for selecting those discontinuities of the function $f(x, y)$ to which the grid will be adapted. Therefore, it is necessary to have one more controlling parameter determining the width of the layer of high gradients that approximates the discontinuity line in the solution and simultaneously restricts maximum gradient of the control function. It is accomplished as follows. First, on the existing grid we define the function $\tilde{f} = c_a f^h$, where f^h is an interpolant of the function f whose value in the nodes coincides

with the value of the function f. When solving the gas dynamics problem, the function f is defined in the center of cells, therefore, we shall update the values of f to the nodes. We apply the simplest interpolation formulae using the area of cells surrounding a given node. Then we specify $D_{\max}$, maximal value of modulus of gradient to the control function f, for example, as $D_{\max} = \lambda \max(|\nabla \tilde{f}|)$, where the coefficient $\lambda < 1$ and $|\nabla \tilde{f}| = \sqrt{\tilde{f}_x^2 + \tilde{f}_y^2}$. Next the gradient of the function is updated as follows

$$\nabla \tilde{f}^* = \begin{cases} D_{\max} \nabla \tilde{f} / |\nabla \tilde{f}| & \text{if } |\nabla \tilde{f}| > D_{\max} \\ \nabla \tilde{f} & \text{otherwise} \end{cases}$$

Then obtained values $\tilde{f}_x^*$ and $\tilde{f}_y^*$ are substituted into Equation (7) instead of f_x and f_y.

It is not necessary to use this procedure in simulation of smooth subsonic flows, however, in the case of supersonic flows we shall apply it to prevent cells to be folded in the vicinity of the shock waves and tangential discontinuities.

If it is necessary to generate the grid with adaptation to the vector-function with components $f_i(x, y)$, the functional Equation (7) can be generalized as

$$I = \int\int \frac{g_{11}(x_\xi^2 + x_\eta^2) + 2g_{12}(x_\xi y_\xi + x_\eta y_\eta) + g_{22}(y_\xi^2 + y_\eta^2)}{(x_\xi y_\eta - x_\eta y_\xi)\sqrt{g_{11}g_{22} - g_{12}^2}} \, \mathrm{d}\xi \, \mathrm{d}\eta$$

where

$$g_{11} = 1 + \sum_i c_i^2 (f_i)_x^2, \quad g_{12} = \sum_i c_i^2 (f_i)_x (f_i)_y, \quad g_{22} = 1 + \sum_i c_i^2 (f_i)_y^2$$

The geometrical meaning of the problem of minimizing the above functional is the following. It is equivalent to the problem of constructing harmonic coordinates on the surface of the graph of the control vector-function with components $r(x, y) = (c_1 f_1, c_2 f_2, \ldots)(x, y)$ (see Reference [13]). The harmonic coordinates are defined using a harmonic mapping of the surface onto the parametric square, see Figure 3. As a result we obtain a parametrization of the surface $(x, y, c_1 f_1, c_2 f_2, \ldots)$ (ξ, η). In case of an unstructured grid we consider the harmonic mapping of every cell on the surface of the vector-function onto the same square cell.

In such an approach the functions $f_i(x, y)$ can be both the gas dynamics values u, v, p, ρ and some function depending on them, for example, $|V| = \sqrt{u^2 + v^2}$. Derivatives of those functions are normalized as above using the corresponding maximal modulus of the gradients $D_{i,\max}$.

5. MINIMIZATION OF THE FUNCTIONAL

The functional can be approximated in such a way that its minimum is attained on a grid of convex quadrilaterals:

$$I^h = \sum_{N=1}^{N_e} \sum_{k=1}^{4} \frac{1}{4} [F_k]_N \tag{11}$$

where

$$F_k = \frac{D_1[1+(f_x)_k^2] + D_2[1+(f_y)_k^2] + 2D_3(f_x)_k(f_y)_k}{J_k[1+(f_x)_k^2+(f_y)_k^2]^{1/2}}$$

$$D_1 = (x_{k-1}-x_k)^2 + (x_{k+1}-x_k)^2, \quad D_2 = (y_{k-1}-y_k)^2 + (y_{k+1}-y_k)^2$$

$$D_3 = (x_{k-1}-x_k)(y_{k-1}-y_k) + (x_{k+1}-x_k)(y_{k+1}-y_k)$$

$$J_k = (x_{k-1}-x_k)(y_{k+1}-y_k) - (x_{k+1}-x_k)(y_{k-1}-y_k)$$

Here $(f_x)_k$ and $(f_y)_k$ are the values of derivatives at node number k of cell number N.

The function I^h possesses the following very important property (see Reference [2]).

> *The function I^h has an infinite barrier on the boundary of the set of unfolded grids, i.e. if at least one of the quantities J_k in Equation* (6) *tends to zero for some cell while remaining positive, then $I^h \to +\infty$.*

From this it follows that if the set of unfolded grids $\mathscr{D}$ is not empty, the system of algebraic equations

$$R_x = \frac{\partial I^h}{\partial x_n} = 0, \quad R_y = \frac{\partial I^h}{\partial y_n} = 0$$

has at least one solution which is an unfolded grid. To find it, one must first find a certain initial unfolded grid, and then use some method of unconstrained minimization of the function I^h. Since this function has an infinite barrier on the boundary of the set $\mathscr{D}$, each step of the method can be chosen so that the grid always remains unfolded (see Reference [12]).

Suppose the grid at the lth step of iterations is determined. We use the quasi-Newtonian procedure when the $(l+1)$-th step is accomplished as follows

$$\begin{aligned} x_n^{l+1} &= x_n^l - \tau\left(R_x\frac{\partial R_y}{\partial y_n} - R_y\frac{\partial R_x}{\partial y_n}\right)\left(\frac{\partial R_x}{\partial x_n}\frac{\partial R_y}{\partial y_n} - \frac{\partial R_y}{\partial x_n}\frac{\partial R_x}{\partial y_n}\right)^{-1} \\ y_n^{l+1} &= y_n^l - \tau\left(R_y\frac{\partial R_x}{\partial x_n} - R_x\frac{\partial R_y}{\partial x_n}\right)\left(\frac{\partial R_x}{\partial x_n}\frac{\partial R_y}{\partial y_n} - \frac{\partial R_y}{\partial x_n}\frac{\partial R_x}{\partial y_n}\right)^{-1} \end{aligned} \tag{12}$$

where τ is the iteration parameter, which can be chosen so that the grid remains unfolded. For this purpose after every step condition (Equation (6)) are checked and if they are not satisfied, this parameter is multiplied by 0.5. Then conditions (Equation (6)) are checked for the grid, computed with a new value of τ and if they are not satisfied, this parameter is multiplied by 0.25 and so on.

As a result the variational method of adaptive-harmonic grid generation has an immanent guarantee to produce grids free of folding at every time step. Computational formulae are described in detail in Reference [2].

Values of derivatives, multiplied by c_a, are recalculated in such a way, that maximum of gradient modulus does not exceed $D_{\max}$ as described in Section 4. Obtained values of derivatives are substituted into computational formulae.

In the case of adaptation to the vector-function we replace $[1 + (f_x)_k^2]$ by g_{11}, $[(f_x)_k(f_y)_k]$ by g_{12}, $[1 + (f_y)_k^2]$ by g_{22}, $\sqrt{1 + (f_x)_k^2 + (f_y)_k^2}$ by $\sqrt{g_{11}g_{22} - g_{12}^2}$. Here g_{11}, g_{12} and g_{22} are computed by using the formulae from Section 4.

6. DYNAMIC SOLUTION-ADAPTIVE COUPLED ALGORITHM

The process of grid generation usually contains preliminary and two main stages. At the preliminary stage coordinates of the boundary points are obtained. At the first stage coordinates of the boundary points are used to compute coordinates of internal nodes. This is an initial grid generation step. Here we use folding-free harmonic grid generation algorithm, ensuring all grid cells to be convex quadrilaterals [2, 12].

At the second stage we perform simulation of the physical process on the grid which can be adjusted to the singularities of the numerical solution with the purpose of increasing the accuracy of computations. Further it is possible to return to the preliminary or first stage if some corrections of the boundary or initial grid are required.

Note the process of grid generation is multi-component and, therefore, different algorithms can be applied at different stages.

One time step to solve the 2D equations of gas dynamics with grid adaptation contains the following stages:

(1) Generate the grid at the next time step. As an initial guess we can either use the grid from the previous time level or, what is the most effective, define the node coordinates by their velocity from the previous time level. Value of time step Δt, defined in Equation (4), is calculated at the previous step from the stability condition.
(2) Compute the gas dynamics values at the next time level using the flow solver described in Section 2.
(3) Update the control function (or vector-function) from the cells centers to nodes. The result is a control function value f_{ij} at every grid node.
(4) Evaluate the derivatives $(f_x)_{ij}$ and $(f_y)_{ij}$ at every grid node.
(5) Make one iteration step and compute the new values of x_{ij} and y_{ij} by formulae (12).
(6) Repeat starting with step (2) to convergence.
(7) Compute the gas dynamics values at the next time level using the flow solver.

To accelerate the adaptation procedure the following algorithm can be applied. At every time step the first main iteration is performed for the entire grid. Next iterations are executed only for those grid nodes which displaced at the main iteration more than 0.1 of maximal value. Solution of the gas dynamics problem is executed for corresponding cells. It allows to decrease the run time about three times.

7. FLOW IN CHANNEL

The method presented here was applied to the well known test of the planar nonstationary supersonic flow in the wind tunnel containing a step [14, 15]. To estimate the accuracy of

numerical solution we use velocity components, pressure and density contours, positions of shocks and their intensity.

The wind tunnel is one unit wide and three units length, step is 0.2 units height and begins at $x = 0.6$, see Figure 4. Initial conditions are $\boldsymbol{f} = (3, 0, 1, 1.4)^T$ that corresponds to the flow-in boundary condition at $x = 0$ as well. Ratio of specific heats $\gamma = 1.4$. The exit boundary has the transmissive conditions since at $x = 3$ the flow is supersonic. Along the walls of the tunnel reflecting boundary conditions are applied.

The process is nonstationary, a steady flow develops only by time 12. However, after time 4 the structure of the flow changes weakly and we shall consider the time evolution up to $t = 4$. The corner of the step is the center of a rarefaction fan and, hence, is a singular point of the flow. Just above the step there is a thin 'boundary layer'. Shock wave interacts with this layer and qualitative nature of the flow near the step is altered. When computing on the rectangular grid we apply the additional boundary condition to the density and velocity near the corner of the step [14] to minimize numerical errors generated by the corner.

In Figure 4(a)–(d) the density contours are shown at time moments $t = 0.5, 1, 2, 4$. Computations were performed on the rectangular uniform 480×160 grid with the spacings $h_x = h_y = 1/160$. Note that in this case and in all further computations the shocks obtained by the first-order scheme are rather thick and they were recognized improper to be presented here. The results in Figure 4 are the same that in Reference [14]. At time $t = 0.5$ (Figure 4(a)) the bow shock is formed, then extending by $t = 1$ it reaches the top wall and reflects from it (Figure 4(b)). In some time, about $t = 2$ (Figure 4(c)), the shock reflects from the step, near the top wall the Mach stem emerges and the contact discontinuity emanates from the triple point. By time $t = 4$ (Figure 4(d)) the shock wave has already reflected triply, the contact discontinuity has intersected twice the shock. Results obtained on such a refined grid we will consider as a standard to estimate the accuracy of calculations on the moving and adaptive grids. Note that if calculating on the rectangular grid without above additional boundary condition, we shall have irregular reflection from the step [16].

In the first set of computations we have studied possibility to increase the accuracy by using the technology of moving grids and consisting of cutting the physical domain into subdomains with boundaries being the shock waves or contact discontinuities. However, in this example it is easy to capture only the bow shock as a boundary line. Attempt to capture the reflecting shocks as the boundary of subdomains runs into serious difficulties since both the boundary of subdomains and their number are changing during the process.

In Figure 5(a),(b) the 150×60 grid and density contours are shown at time $t = 4$. When calculating we apply the shock-fitting procedure to capture the bow shock and Mach stem without using the grid adaptation procedure. An additional boundary condition imposed near the corner of the step [14] on such a curvilinear grid leads to increasing the errors caused by the corner influence and we do not apply it. Nevertheless, we obtain the reflection from the step similar to that obtained on the rectangular grid with applying that boundary condition. Thus, using the proper grid conforming with the solution, when the grid lines align with the stream lines near the corner, enables the reduction of those numerical errors. We can estimate the error comparing the results shown in Figure 5(b) with standard results from Figure 4(d). It can be seen that the thickness of the reflected shock wave is about three to four times larger as for the standard.

In order to increase the accuracy in the next set of computations we have used the grid adaptation together with the shock fitting procedure.

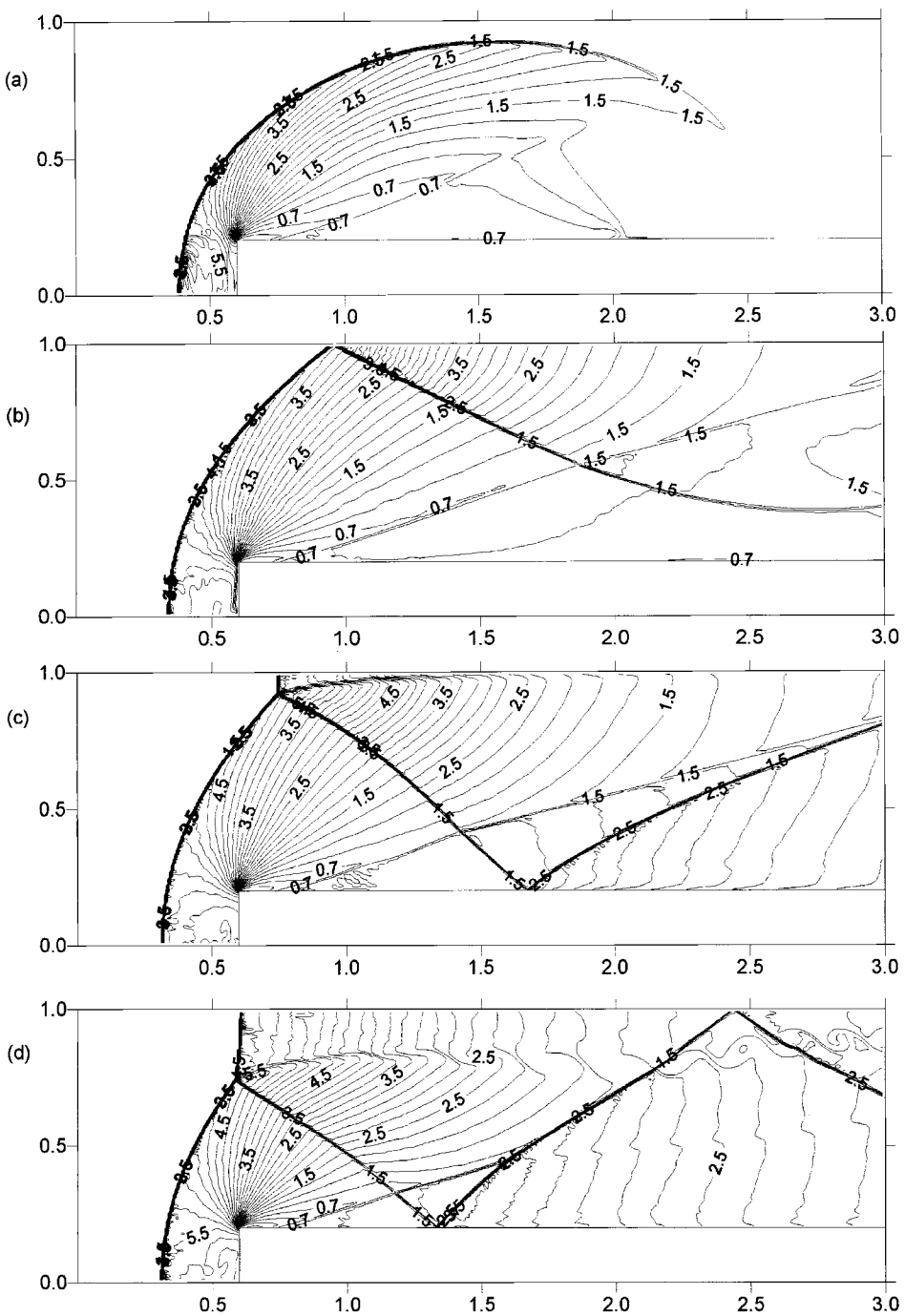

Figure 4. Density contours at (a) $t = 0.5$, (b) $t = 1$, (c) $t = 2$, (d) $t = 4$, on the uniform rectangular 480×160 grid.

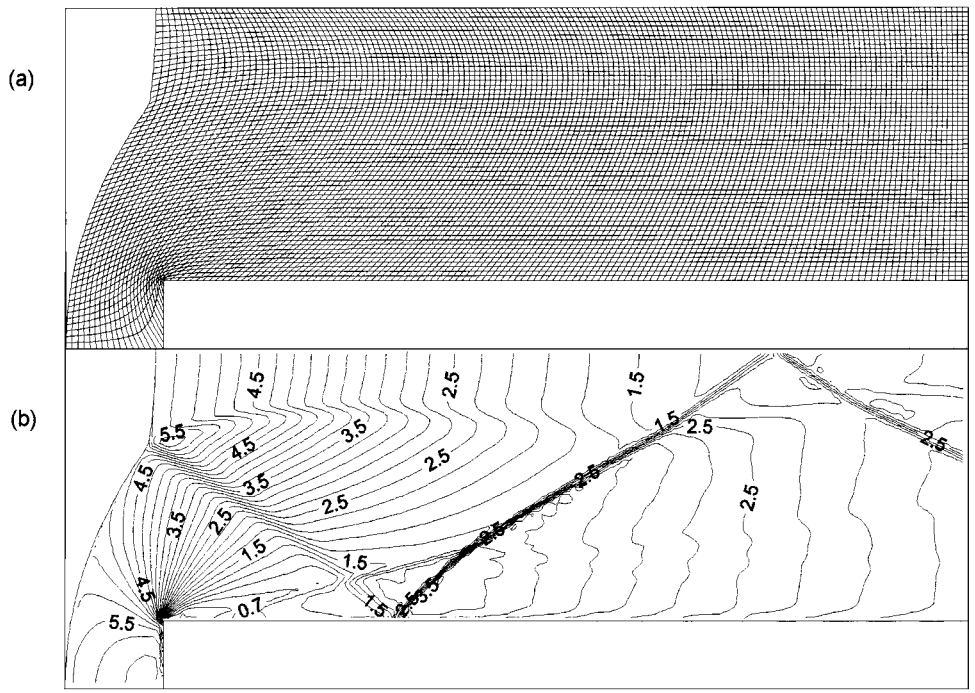

Figure 5. Moving quasiuniform 150×60 grid (a) applied together with the shock-fitting procedure to the left bow shock and Mach stem at $t = 4$; density contours (b).

First, we have performed computations with adaptation to the vector-function $(u, v, p, \rho)^T$. The adapted grid at $t = 4$ and u, v, p, ρ contours are shown in Figure 6. The adaptation procedure was switched on at time 3.95, before this the calculations were performed only with fitting the bow shock. Since time 3.95 every time step includes one additional iteration for the grid and during it we solve the gas dynamics problem for the entire grid. Thus, the total number of iterations for the grid at every time step N_{iter} was equal to 2. Adaptation was performed along the boundaries as well, including the moving bow shock, with the use of a 1D algorithm [12]. The iteration parameter $\tau = 0.15$, coefficient of adaptation was defined as follows:

$$c_a = \begin{cases} 0.2 & \text{if } x \leqslant 0.6 \\ 0.2 - 0.05(x - 0.6)/(3 - 0.6) & \text{if } x > 0.6 \end{cases}$$

and for each component of the vector-function $c_i = 0.25 c_a$, coefficient $D_{\max} = 100$ in all variants. We can see that grid lines compression to the shock wave emanating from the triple point is strong enough meanwhile the contact discontinuity is weakly indicated. Disturbances from the corner distort strongly the grid cells and we had to decrease c_a down to 0.05 in the vicinity of the point where the shock wave reflects from the step. Otherwise we would get distorted cells. Furthermore, we switched off adaptation ($c_a = 0$) in the vicinity of the corner in all variants since the rarefaction wave affects the shape of cells in the same manner.

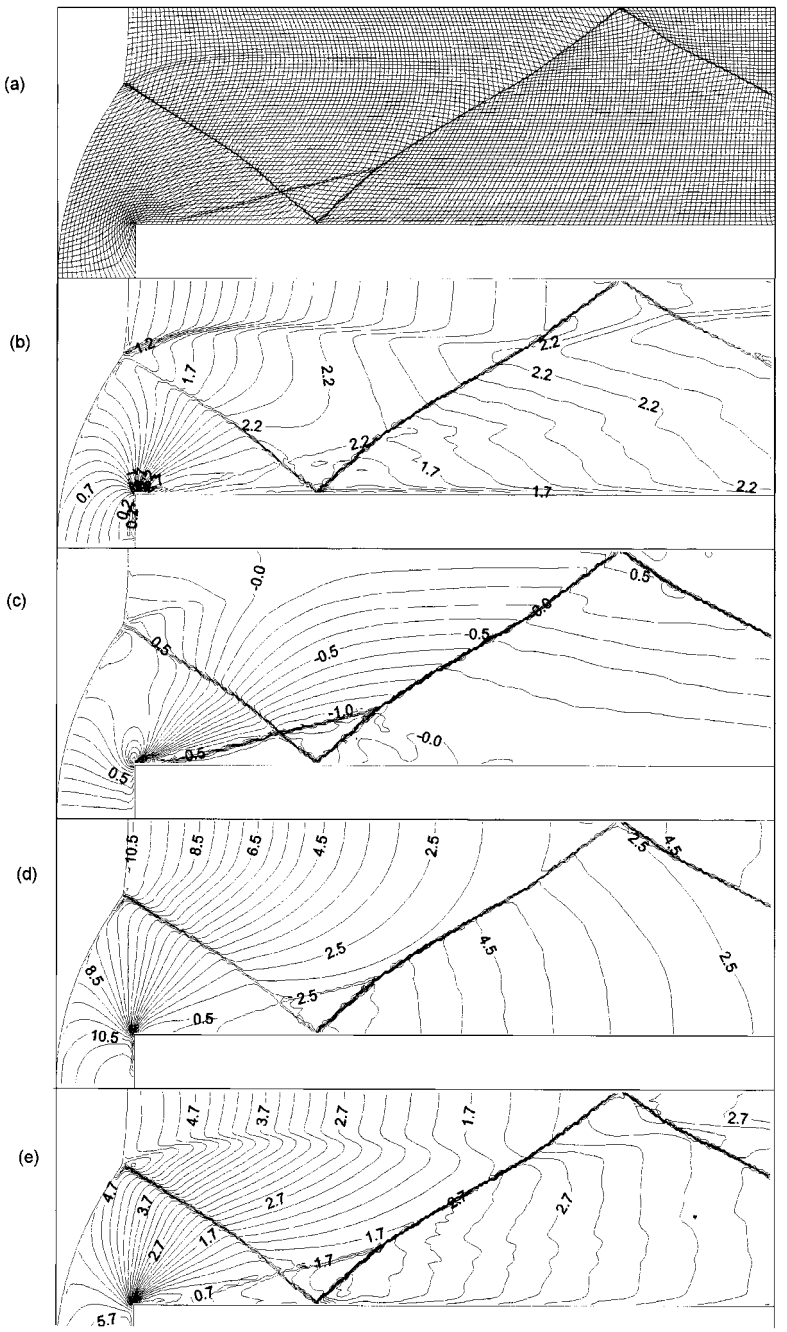

Figure 6. Adaptive 150×60 grid (a) applied together with the shock-fitting procedure at $t = 4$; velocity components u (b) and v (c), pressure (d) and density (e) contours. Adaptation to the vector-function $(u, v, p, \rho)^T$.

Results of computations with adaptation to scalar functions ρ and $|V|$ are presented in Figure 7(a) and (b), correspondingly. Contours of $|V|$ are presented in Figure 7(c). Fragment of the grid from Figure 7(b) is shown in Figure 7(d). Coefficient of adaptation c_a was defined as above. In the case of adaptation to ρ the grid does not 'feel' the contact discontinuity, but in the case of adaptation to $|V|$ the grid compression to the contact discontinuity was obtained. Comparing Figure 6(e) and Figure 7(c) we can see that the reason lies in different behavior of the ρ and $|V|$ contours in the vicinity of the contact discontinuity.

We see that computations including adaptation coupled with the shock-fitting procedure have been quite successful. It can be recommended in various applications where the bow shocks can be captured as boundary lines.

An easy way to obtain nearly the same resolution is to perform global adaptation without shock fitting.

In the next calculations with global adaptation the grid has been adapted to the vector-function $(u, v, p, \rho)^T$. Figures 8 and 9 present the grids and density contours at the same time moments as in Figure 4. The main calculation was performed with $N_{\text{iter}} = 2$, $D_{\max} = 5$ and $c_a = 0.1$. In order to increase the accuracy at 0.05 before every time point the adaptive parameters were changed to:

(1) $t = 0.5$ (see Figure 8(a),(b)) $N_{\text{iter}} = 10$, $D_{\max} = 100$, $c_a = 0.075$,
(2) $t = 1$ (see Figure 8(c),(d)) $N_{\text{iter}} = 6$, $D_{\max} = 100$

$$c_a = \begin{cases} 0.075 & \text{if } x \leqslant 1 \\ 0.075 + 0.175(x-1)/(3-1) & \text{if } x > 1 \end{cases}$$

(3) $t = 2$ (see Figure 9(a),(b)) $N_{\text{iter}} = 4$, $D_{\max} = 100$

$$c_a = \begin{cases} 0.05 & \text{if } x \leqslant 0.8 \\ 0.05 + 0.15(x-0.8)/(1.5-0.8) & \text{if } 0.8 < x < 1.5 \\ 0.2 & \text{if } x > 1.5 \end{cases}$$

(4) $t = 4$ (see Figure 9(c),(d)) $N_{\text{iter}} = 2$, $D_{\max} = 100$

$$c_a = \begin{cases} 0.05 & \text{if } x \leqslant 0.6 \\ 0.05 + 0.15(x-0.8)/(1-0.6) & \text{if } 0.6 < x < 1 \\ 0.2 & \text{if } x > 1 \end{cases}$$

For each component of the vector-function $c_i = 0.25 c_a$. The choice of different values of N_{iter} is caused by the different speed of the flow evolution.

We were forced to pay particular attention to the subdomain where the grid lines 'formed' the triple point, see Figure 9(a),(c), since it is a very sensitive place and large value of c_a can cause the grid lines to overlap. One more way to prevent grid folding in this subdomain is to decrease temporally the iteration parameter τ when the triple point is being formed.

The contours of u, v, p, ρ at $t = 4$ are presented in Figure 10. As in computations with shock-fitting (see Figure 7(b)) we expect the grid will condense strongly to the tangential discontinuity with $|V|$ as an adaptation criterion. Parameters of adaptation in this case were defined as above. The grid, ρ, $|V|$ contours and fragment of the grid at $t = 4$ are shown

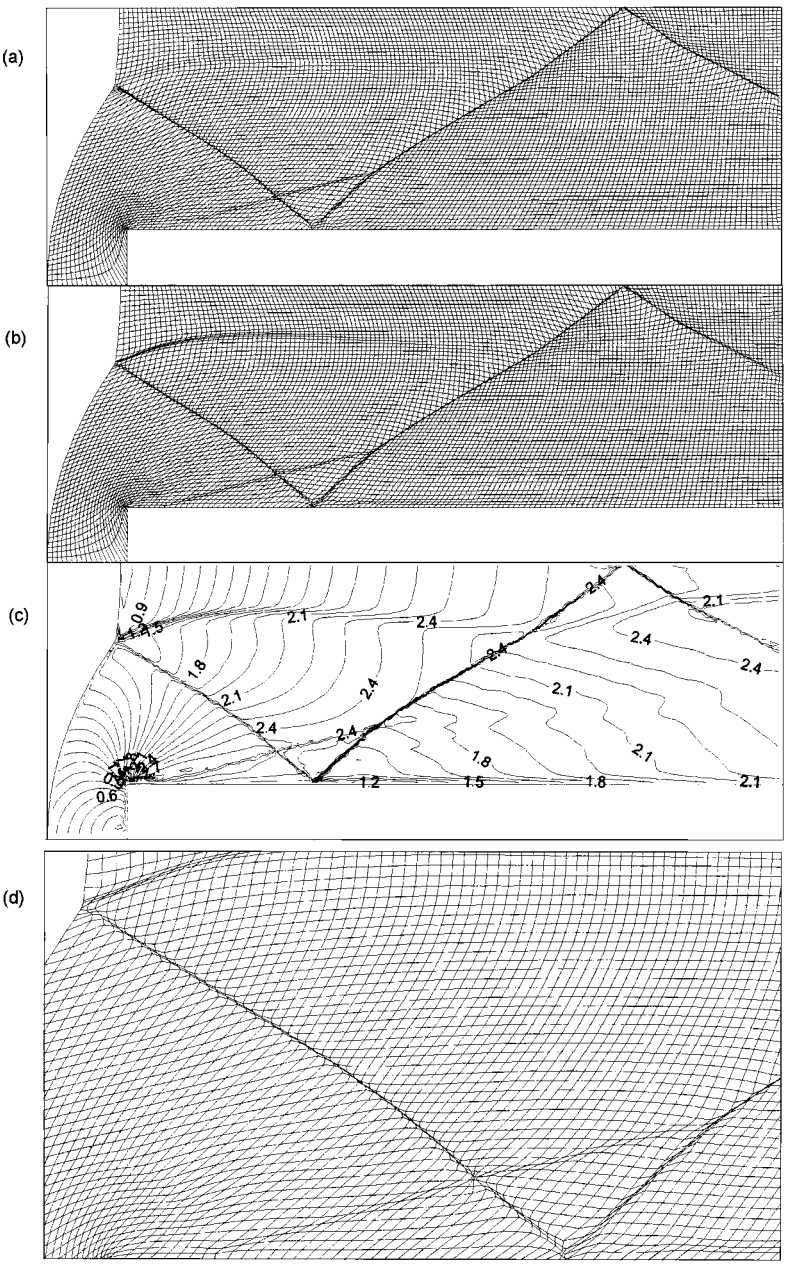

Figure 7. Adaptive 150×60 grids at $t = 4$ applied together with the shock-fitting procedure when adapting to ρ (a) and $|V|$ (b) as a control function; $|V|$ contours (c) in the second case and fragment of the grid (d).

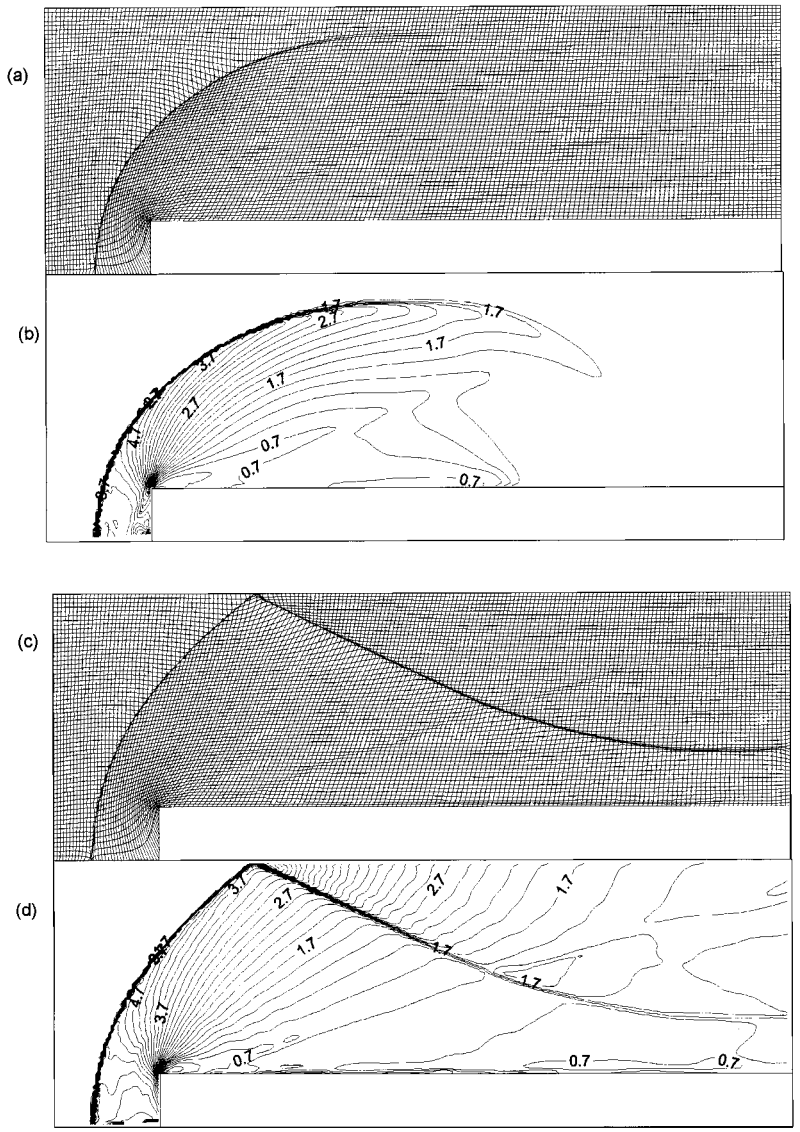

Figure 8. Global adaptation. Adaptive 180×60 grids and density contours at $t = 0.5$ (a,b) and 1 (c,d). Adaptation to the vector-function $(u, v, p, \rho)^T$.

in Figure 11. On the whole, due to grid adaptation the shock waves thickness decreases greatly. In the fragment of the grid, Figure 11(c), we see all the shocks are indicated by very compressed grid lines. Accuracy of computations increases due to the appearance of the very narrow stretched cells in the vicinity of the bow shock, Mach stem and reflected shocks. Maximal aspect ratio achieves 50. Approximately by this factor the width of smearing of the shocks is decreased. This can cause the accuracy of numerical solution to be increased by

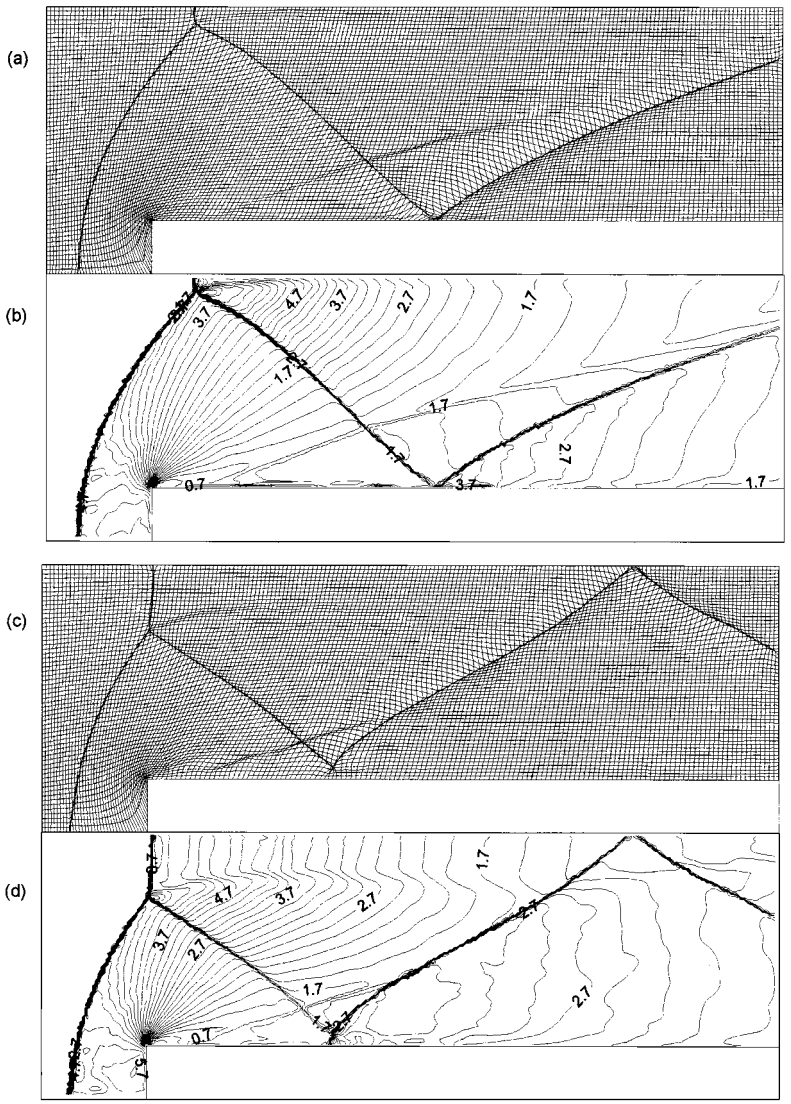

Figure 9. Global adaptation. Adaptive 180×60 grids and density contours at $t = 2$ (a,b) and $t = 4$ (c,d). Adaptation to the vector-function $(u, v, p, \rho)^T$.

several times [17]. Presence of distorted cells in the vicinity of the shock wave, emanating from the triple point, probably influences the quality of the solution insignificantly. In the region where the shock reflects from the step, Figure 11(a), the line of nodes clustering is a bit distorted due to the mentioned numerical boundary layer and as above we set here $c_a = 0.05$.

Performed computations confirm the presence of an additional smoothing. When using an adaptive grid the coordinate lines align along the shock waves, forming the stretched cells oriented along the shocks. The amplitude of spurious oscillations is decreased by several

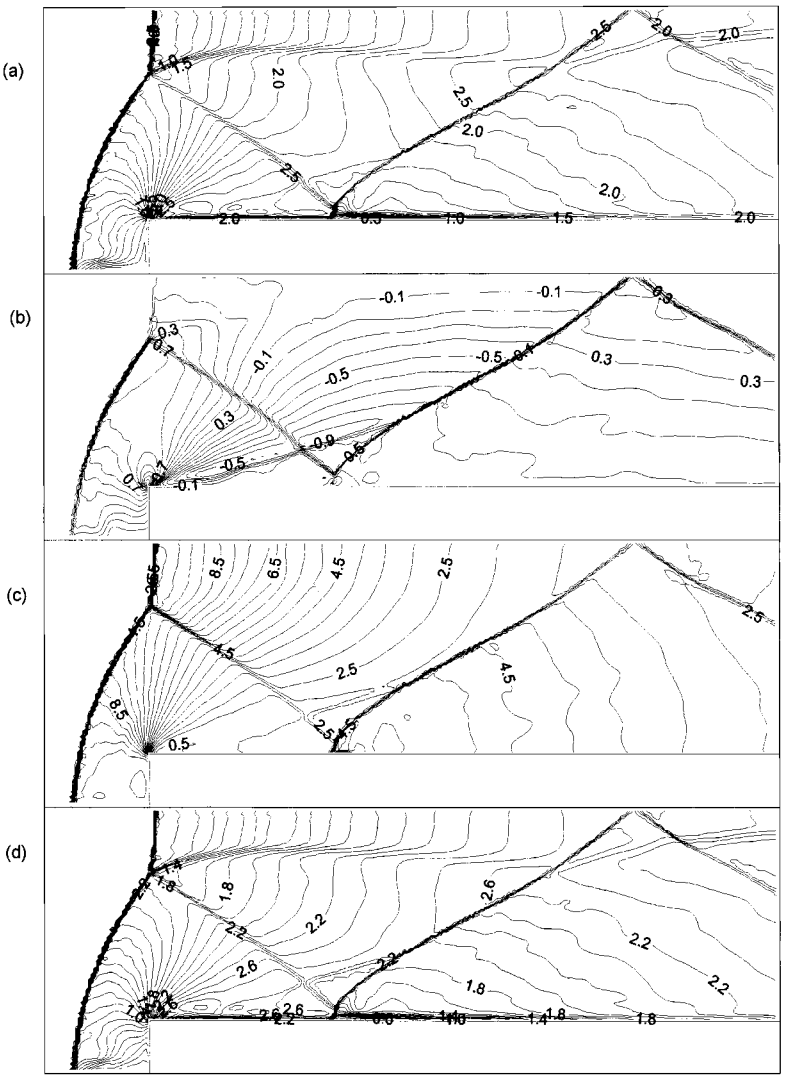

Figure 10. Global adaptation. Velocity components u (a) and v (b), pressure (c) and $|V|$ (d) contours at $t = 4$. Adaptation to the vector-function $(u, v, p, \rho)^T$.

factors of 10 in comparison with the results obtained on the rectangular grid, see Figure 4(d) and Figures 9(d) and 11(b).

8. CONCLUDING REMARKS

Results of computations presented in this paper show that the method of adaptive-harmonic grid generation can be successfully applied to nonstationary problems of gas dynamics.

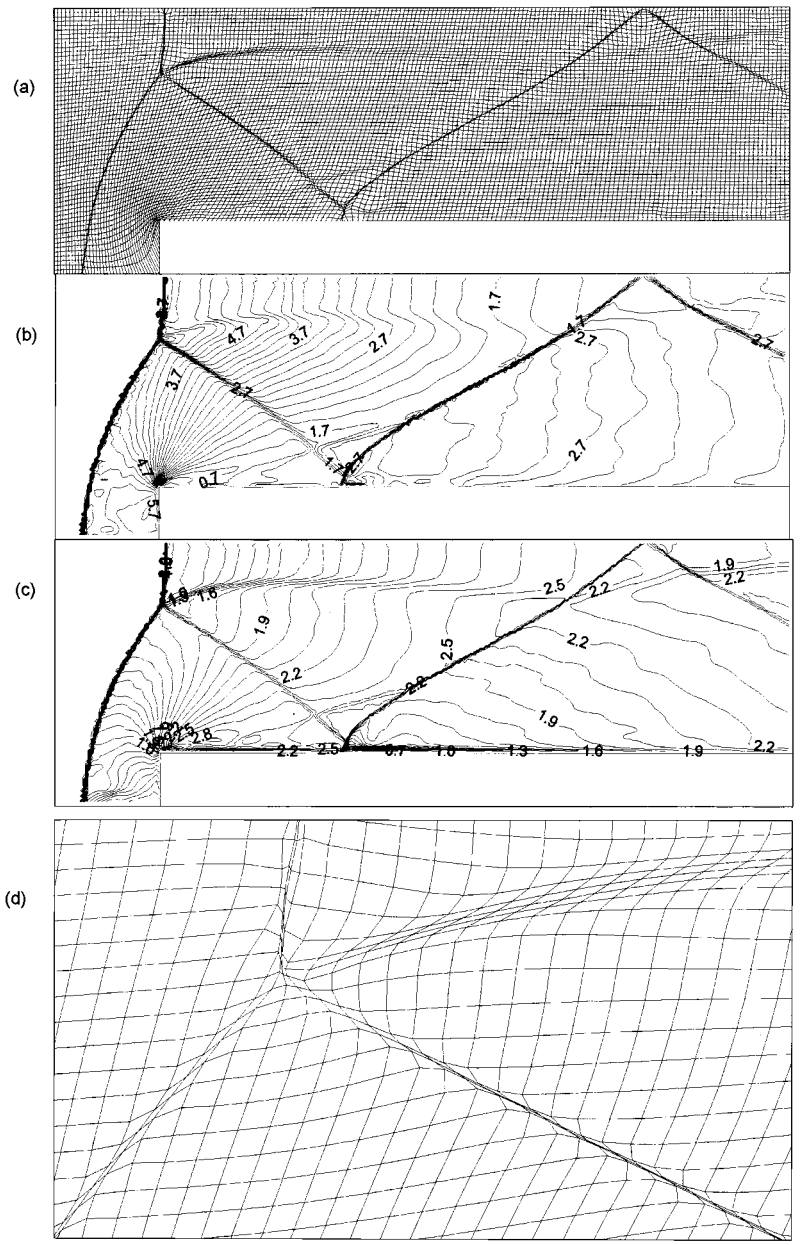

Figure 11. Global adaptation with $|V|$ as an adaptation criterion. Adaptive 180×60 grid (a), density (b) and $|V|$ (c) contours at $t = 4$. Fragment of the grid in the vicinity of the triple point (d).

The main conclusion is the following. In nonstationary problems it is necessary to use special procedures in adaptation algorithm to prevent grid folding. Our experience has shown that in the case of high compression of grid lines, the property to produce grids free of folding

is the most important. The present method is based on minimization of the functional with infinite barrier on the boundary of the set of grids with all convex cells and this guarantees unfolded grid generation during computations at every time step.

Another important question discussed in many papers is the choice of adaptation criterion. Our experience has shown that it is better to start with common criterion, i.e., to perform adaptation to the vector-function of all dependent variables $(u, v, p, \rho)^T$. Then we can adjust coefficients of adaptation c_i separately to achieve better resolution of singularities.

The grid is clustered in such a way that we can obtain quite a satisfactory resolution of the shocks with not a great number of grid nodes. For the above test the accuracy on the adaptive grid is higher, due to decreasing the thickness of shocks, than on the rectangular grid with a greater number of nodes by a factor of 7.1. At the same time in case of adaptation it is required less run time by a factor of 1.5. Note the method is not quite automatic. Success of adaptation depends on the coefficient of adaptation c_a to be selected during computations.

As in the case of a uniform grid, here the shock wave is smeared within three cells and the grid with strong clustering looks like a set of blocks with the boundaries defined automatically as the lines of grid nodes clustering. Inside every 'block' the grid is quasiuniform and the solution is smooth. This approach may be considered as a further development of the moving block technology presented in the monograph [11], where the flow domain is divided into blocks with boundaries being the shock waves or contact discontinuities.

The advantage of the moving adaptive grid technology is that such a 'cutting' is performed automatically. In real-world computations we can obtain such a complex nonstationary configuration of the blocks that even if we would be able to capture their boundaries 'by hand', we will have serious problems in attempting to join those blocks. In complex situations it is necessary to adjust the parameters of the algorithm to provide both unfolded grid generation at every time step and smooth variation of the grid control parameters. For example, at Mach stem emerging in the vicinity of the triple point strongly distorted cells appear up to their degeneration. Hence, in this subdomain we shall not specify too large a value of c_a.

Formally moving adaptive-harmonic grid generation method can be extended to the 3D case [2], however, it is necessary to perform additional theoretical and experimental investigations with the purpose of creating algorithms with an immanent guarantee of producing grids free of folding.

REFERENCES

1. Ivanenko SA. Adaptive-harmonic grid generation and its application for numerical solution of the problems with boundary and interior layers. *Computational Mathematics and Mathematical Physics* 1995; **35**(10):1203–1220.
2. Ivanenko SA. Harmonic mappings, Ch. 8. *Handbook of Grid Generation*. CRC Press: Boca Raton, FL, 1999.
3. Ivanenko SA, Muratova GV. Adaptive grid shallow water modeling. *Applied Numerical Mathematics* 2000; **32**(4):447–482.
4. Thompson JF, Soni BK, Weatherill NP (eds). *Handbook of Grid Generation*. CRC Press: Boca Raton, FL, 1999.
5. McRay DS, R. Laflin KR. Dynamic grid adaptation and grid quality, Ch. 34. *Handbook of Grid Generation*. CRC Press: Boca Raton, FL, 1999.
6. Thompson JF. A survey of dynamically-adaptive grids in the numerical solution of partial differential equations. *Applied Numerical Mathematics* 1985; **1**:3–27.
7. Ingram CL, McRay DS. Extension of a dynamic solution-adaptive grid algorithm and solver to general structured multi-block configurations, AIAA 96-0294, AIAA 34th Aerospace Science Meeting, Reno: NV, Jan. 1996.
8. Zegeling PA. Moving grid techniques, Ch. 37. *Handbook of Grid Generation*. CRC Press: Boca Raton, FL, 1999.
9. Liu F, Ji S, Liao G. An adaptive grid method and its application to steady Euler flow calculations. *SIAM Journal of Scientific Computing* 1998; **20**:811–825.

10. Azarenok BN. Realization of a second-order Godunov's scheme. *Computer Methods in Applied Mechanics and Engineering* 2000; **189**(3):1031–1052.
11. Godunov SK, Zabrodin AV, Ivanov MY, Kraiko AN, Prokopov GP. *Numerical Solution of Multi-dimensional Problems in Gas Dynamics*. Nauka Press: Moscow, 1976.
12. Charakhch'yan AA, Ivanenko SA. A variational form of the Winslow grid generator. *Journal of Computational Physics* 1997; **136**:385–398.
13. Liseikin VD. *Grid Generation Methods*. Springer-Verlag: New York, 1999.
14. Colella P, Woodward PR. The numerical simulation of two-dimensional fluid flow with strong shocks. *Journal of Computational Physics* 1984; **54**:115–173.
15. Kim C, Jameson A. A robust and accurate LED–BGK solver on unstructured adaptive meshes. *Journal of Computational Physics* 1998; **143**:598–627.
16. Woodward PR, Colella P. *Lectures Notes in Physics No. 141*, Springer-Verlag: New York/Berlin, 1981: 434.
17. Azarenok BN. Adaptive moving grids in supersonic flow simulation. In *Numerical Grid Generation in Computational Field Simulations*, *Proceedings of the 7th International Conference*, September 25–28, 2000, Whistler, British Columbia. Soni BK, Haeuser J, Thompson JF, Eiseman P (eds). 2000: 629–638.

